Journal of Materials Chemistry C

ROYAL SOCIETY OF CHEMISTRY

PAPER

View Article Online
View Journal

Cite this: DOI: 10.1039/d5tc01610j

Laser-induced kirigami structures of liquid crystal elastomers for multimodal morphing†

Bing Lei,[ab] Lei Huang,[a] Ke-Hui Wu,[a] Rui Zhou[de] and Lu-Jian Chen *[ac]

Received 21st April 2025,
Accepted 3rd July 2025

DOI: 10.1039/d5tc01610j

rsc.li/materials-c

Kirigami offers a versatile framework for transforming planar films into three-dimensional (3D) intricate structures, which is instrumental in developing liquid crystal elastomer (LCE) soft robots. These robots can dynamically alter their shapes to accommodate various functionalities. By meticulously designing the geometries of cuts, a range of out-of-plane configurations can be induced, resulting in an expanded repertoire of deformation modes. In this study, we utilize a commercially available laser engraver for the precise alignment of anisotropic kirigami azobenzene (azo) LCEs, streamlining the manufacturing process of cuts with diverse geometric shapes. The resulting actuators possess a predetermined alignment within defined geometric regions, enabling them to exhibit a variety of complex shapes when stimulated by light. Furthermore, polyimide (PI) films can be selectively transformed into graphene-coated films through surface carbonization using the 450 nm laser from the engraver, resulting in bilayer kirigami structures with enriched shape-changing capabilities. These highly maneuverable soft actuators demonstrate distinct functionalities, such as grasping and transporting micro-cargo. We anticipate that the evolution of intelligent soft robotics, characterized by multimodal morphing and seamless functional integration, will be propelled by laser-induced kirigami azo-LCEs.

Introduction

Liquid crystal elastomers (LCEs) are interconnected polymer networks with the flexibility of rubber and the inherent anisotropy of liquid crystals (LCs), which endow LCEs with unique physical and optical properties, including mechanical propulsion, flexible resilience, and optical birefringence.[1–8] The outstanding physical and optical properties exhibited by LCEs depend on the interplay of cross-linking and alignment techniques applied in the polymer network to the liquid crystal mesocrystals. The regulating liquid crystal alignment is crucial for coordinating the soft propulsive deformation dynamics formulated by the LCEs.[9] The dominant alignment methods for the LCEs are broadly categorized into four different types: mechanical alignment, surface-enforced alignment, field-assisted alignment, and rheological alignment.[10] It is worth noting that the surface-enforced alignment method has been widely adopted due to its precise indication of the direction and ease of establishing pattern alignment. The research design of soft actuators, based on surface-enforced alignment methods, culminates in shape changing and kinetic responses, including bending, twisting, and buckling, all of which are induced by external stimuli, such as light, humidity, and temperature.[11–16] Particularly noteworthy is the fact that with the advent of various light sources, such as light-emitting diodes (LEDs) and laser diodes (LDs), as well as the development of components to modulate light, such as digital micromirror devices (DMDs) and liquid crystals on silicon (LCOS), novel projection and laser direct writing (LDW) techniques have facilitated the development of LCEs with pattern-alignment functionality, and have opened up new possibilities for complex deformations.[17–20]

The deformation mechanism of LCEs depends not only on the control of the internal arrangement of the LC, but is also closely related to the geometry of the LCE. Therefore, in addition to alignment, the shape of the LCE is a key consideration.[21] In this context, kirigami emerges as a captivating paradigm that endows planar entities with three-dimensional (3D) configurations, attracting considerable attention in both scientific and technological fields. Applications encompass deployable configurations for solar panels, biomedical implements, and microelectromechanical systems (MEMS).[22–26] Recently, the integration of kirigami structures into the shaping of LCE films has attracted great attention.[27–33] Through manipulation enabled by kirigami,

[a] Department of Electronic Engineering, School of Electronic Science and Engineering, Xiamen University, Xiamen, 361102, China. E-mail: lujianchen@xmu.edu.cn
[b] School of Physics and Chemistry, Hunan First Normal University, Changsha, 410205, China
[c] Fujian Key Laboratory of Ultrafast Laser Technology and Applications, Xiamen University, Xiamen, 361102, China
[d] Pen-Tung Sah Institute of Micro-Nano Science and Technology, Xiamen University, Xiamen, 361005, China
[e] Innovation Laboratory for Sciences and Technologies of Energy Materials of Fujian Province (IKKEM), Xiamen, 361005, China

† Electronic supplementary information (ESI) available. See DOI: https://doi.org/10.1039/d5tc01610j

these films can exhibit out-of-plane deformations induced by external stress fields in liquid crystal networks. With the help of a laser engraving machine, Chen *et al.* designed and integrated topological defects in aligned LCE microstructures with various geometric shapes towards a single-layer multimodal morphing kirigami actuator.[34] Moreover, the bilayer structure of the composite photothermal layer in LCE makes further shape tuning possible.[35,36] For example, polyimide (PI) films can be laser carbonized into graphene films and used as a photothermal layer by rapidly generating heat under light irradiation at specific wavelengths. The preparation of laser-induced graphene (LIG) films has been widely investigated due to the easy availability of PI films and their extensive range of applications.[37–40] Unfortunately, the photothermal properties of LDW-based LIG layers have not yet been used to induce deformation in the bilayer structure of LCE films, limiting the application of lasers in guiding multimodal deformation of kirigami LCEs.

To address this challenge, we present a streamlined fabrication strategy that capitalizes on the intrinsic advantages of a commercially available laser engraver. This approach not only facilitates the precise alignment and cutting of anisotropic kirigami patterns in azobenzene (azo) LCEs but also offers a unique capability for laser carbonization treatment. Consequently, we can fabricate bilayer carbonized kirigami azo-LCE structures on a single material platform, merging mechanical and optical functionality, adding deformation modulation to the thickness, expanding a new deformation dimension for the anisotropic response under kirigami azo-LCE geometrical constraints. The resulting azo-LCE films exhibit a diverse range of shape transformations, including bending, twisting, dimpling, rotating, and waving. These deformations can be triggered by light, enabling programmable 3D shape transformations. This property allows for the development of bending actuators capable of manipulating objects and crawling robots that demonstrate complex rotational and curvilinear motion capabilities. We anticipate that this laser-induced kirigami design approach has promise for advancing soft robotics with multiple morphing capabilities and integrated functionality. It also provides valuable insights for the further exploration of agile systems.

Experimental

Materials

The azo-LCE mixture (Fig. S1, ESI†) is composed of reactive mesogens (RMs, 90.2 wt%, HCCH), azobenzene (C9-azo, 8.8 wt%, Beijing Fusion Venture Technology Co.) and photoinitiator (Irgacure 819, 1 wt%, Sigma-Aldrich). RMs were made up of RM006, RM021, RM82, and RM257, with a weight ratio of 2.9 : 1 : 1 : 1 : 1, respectively. The material ratios were carefully optimised in our experiments, in particular, the 8.8 wt% of C9-azo ensured the flexibility of the polymer network (polymer network flexibility regulation, ESI†). SD1 molecules (Beijing Fusion Venture Technology Co.) were used to align the liquid crystal molecules. 20 μm PI tape (consisting of a 12.5 μm PI film and a 7.5 μm adhesive silicone layer) was used as the material for carbonization, and the micro-cargo consists of a white cotton ball made from cellulose fibers.

Preparation of the kirigami azo-LCE soft actuators

SD1 molecules were spin-coated onto two indium tin oxide (ITO) glass substrates, which were then bonded together using double-sided electrical tape with a thickness of 40 μm to form a LC cell. Patterned irradiation of the LC cell was carried out using a 450 nm laser engraver (L2, LaserPecker, laser power: 1.98 W, scanning speed: 3.50 mm s^{-1}) to prepare the photoalignment layer. The premixture was introduced into the LC cell by capillary action at an elevated temperature above the clearing point (69 °C). The cells were then cooled to 65 °C to enter the LC phase. Subsequently, the LC cells were placed on a heating table at 65 °C and polymerized with a 405 nm LED (70 mW cm^{-2}) for approximately 15 min. The LC cell was carefully opened using a blade, exposing the surface irradiated for cutting. The same engraver (laser power: 2.50 W, scanning speed: 2.17 mm s^{-1}) was then employed to scan the boundary lines corresponding to the alignment pattern, facilitating the cutting of the desired kirigami pattern.

Preparation of the bilayer kirigami azo-LCE soft actuators

The azo-LCE films were prepared following the previously described procedure. Subsequently, 20 μm thick polyimide (PI) tape was applied to the densely cross-linked surface of the azo-LCE film. A laser engraver (L2, LaserPecker, laser power: 0.99 W, scanning speed: 2.17 mm s^{-1}) was employed to scan and carbonize the designated area. The fabrication process was completed by scanning and cutting the film using the same engraver, according to the desired kirigami shape, to create the bilayer kirigami azo-LCE soft actuators.

Characterization

Actuation of the azo-LCE films was performed using unpolarized UV 365 nm (460 mW cm^{-2}) and visible 460 nm (150 mW cm^{-2}) light from a multichannel LED (Prior Scientific). The carbonized bilayer azo-LCE is driven by an 808 nm fiber-coupled laser (14808F02FN-2.500 W, BWT). Optical images and movies were recorded by using a digital camera (Meiruishi). Polarizing optical microscopy (POM) images were acquired using a microsystem (DM750P, Leica) equipped with a digital camera (E3ISPM20000KPA, Sony). Scanning electron microscopy (SEM) images were obtained using a desktop scanning electron microscope (TM3000, Hitachi). Raman spectra were measured using a Raman spectrometer (Inspector Raman 785, DelteNu). The surface temperature of the actuator before and after 808 nm laser irradiation was measured with an infrared thermometer (FLIR One).

Results and discussion

Laser engraving platform

As shown in Fig. 1a, the 450 nm laser engraver can be used for integrating the alignment microstructures and kirigami

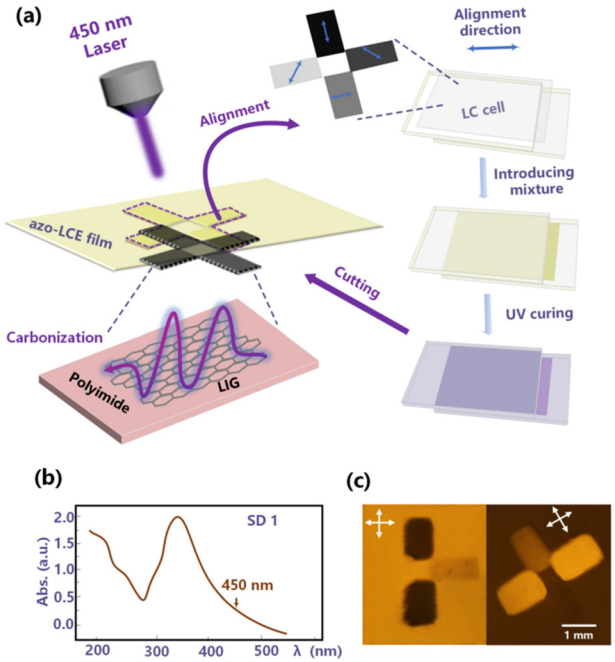

Fig. 1 (a) Manufacturing streamlined alignment microstructures and kirigami geometric shapes for azo-LCE actuators, as well as the carbonization of commercial PI films by a 450 nm laser engraver. (b) Absorption spectra of SD1. (c) POM images of azo-LCE showing birefringence caused by patterned photoalignment using a 450 nm laser engraver.

geometries of LCEs. Additionally, it can also be utilized to carbonize PI films into graphene. To achieve local alignment of the liquid crystal molecules, we modified the engraver by installing a half-wave plate to control the linear polarization angle of the laser (Fig. S2, ESI†). The photosensitive azo-dye for liquid crystals we used is SD1, as shown in Fig. 1b. Although the absorption peak of SD1 is not at 450 nm, the light power of the laser engraver is sufficiently high such that the long-axis of the SD1 molecules can be successfully altered by the incident laser with polarization properties, thus orienting the azo-LCE perpendicular to the direction of the polarized laser. By examining the alignment effect of azo-LCE, we determined the alignment parameters of the engraver, including engraving speed and laser power. As shown in Fig. S3 (ESI†), for the photoresponsive azo-LCE, when the light power of the engraver was 1.98 W and the scanning speed was 3.50 mm s^{-1} with one pixel per step, we observed pronounced alignment in azo-LCE. It is noteworthy that the oriented region of Fig. S3 (ESI†) also shows distinct lines, which may be due to the energy gradient at the edge of the laser spot resulting in a micro-regional change in the alignment direction induced by the SD1 molecules, resulting in the formation of alignment-defective lines along the scanning direction as it transitions from the scanning direction to the perpendicular direction (lines in laser orientation, ESI†). The POM images of azo-LCE showing birefringence caused by patterned photoalignment using a 450 nm laser can be seen in Fig. 1c. After polymerization, we carefully reconfigured the engraver's cutting parameters, which included calibrating the cutting laser power and cutting speed. The introduced cutting pattern corresponded precisely to the alignment template. At a laser power and cutting speed of 2.50 W and 2.17 mm s^{-1}, respectively, the cuts are neat and do not ablate neighboring parts of the sample (Fig. S4, ESI†). It is worth noting that azo molecules are incorporated into the kirigami actuator to achieve optical switching, and it can undergo a transformation from *trans* to *cis* form under 365 nm illumination, thus enabling macroscopic deformation. Moreover, under 460 nm visible light irradiation, azo molecules can undergo a transformation from *cis* to *trans*, thus restoring the deformation. The absorption spectra of the C9-azo molecules in ethanol are shown in Fig. S5 (ESI†). And the absorption spectra of the *cis-trans* isomeric molecule in ethanol match the absorption spectra of the *cis-trans* isomeric molecules in the experimental films.

Rectangular arm single-layer kirigami azo-LCE soft actuators

Azo-LCE films with different alignment microstructures were cut into rectangular geometries with four arms, resulting in multiple deformation modes (Fig. 2). Our previous studies have shown that azo-LCE films have excellent mechanical properties that make them highly foldable and deformable.[41] In addition, the phenomenon of crosslink density gradient in azo-LCE film thickness is inevitable due to the UV absorption property of azobenzene during photopolymerisation. The crosslink density of the film on the side near the UV light is higher than that on the side away from the UV light, which leads to a different modulus of elasticity between the two sides of the film, thus obtaining the deformation characteristic of the film bending from the high cross-linking side to the weakly cross-linking side under UV irradiation (Fig. S6, ESI†). Most importantly, the mechanical behavior of the LC molecule in kirigami is robustly dependent on the combination of local geometrical and anisotropy of the LC director field. In Fig. 2a, the four-armed kirigami LCE soft actuator produces a deformation pattern characterized by bending under UV irradiation (365 nm, 460 mW cm^{-2}) when LC molecules are aligned along the long sides of the rectangular arms. When the orientation of the LC director deviates by 45° from the elongated geometric axis of the rectangular arms, as depicted in Fig. 2b, this results in a deformation that is aptly described as twisting. When the direction of the LC director is perpendicular to the long sides of the rectangular arms, dimpling deformation occurs. We enriched the deformation form of the four arms by setting one pair of opposing arms as dimpling deformation and the other pair to undergo bending deformation (Fig. 2c). In particular, as shown in Fig. 2d, further oriented microstructural partitioning design leads to alternating bending, twisting and dimpling deformation of the four arms (Movie S1, ESI†).

The alignment of azo-LCE kirigami configurations enables the achievement of diverse functionalities based on the resultant shape changes. One such functionality is the bending actuator, which is commonly used in grippers. These grippers typically consist of one or more bending actuators that can respond to external stimuli. We engraved four rectangular azo-LCE strips in a film, each with LC molecules aligned perpendicular to the long side of the rectangular strip, thereby creating a

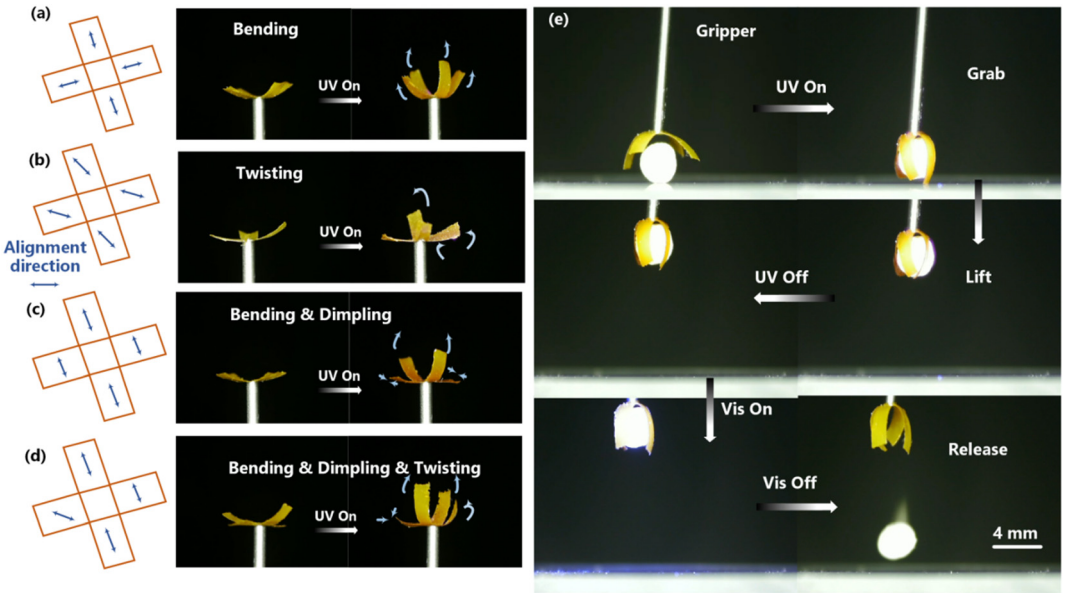

Fig. 2 Multimodal shape morphing of a rectangular four-arm kirigami azo-LCE actuator under various alignment microstructures. Single deformation mode of (a) bending and (b) twisting. (c) Deformation combination of bending and dimpling. (d) Alternating deformations of bending, twisting, and dimpling. (e) Grabbing and releasing object by a rectangular four-arm kirigami azo-LCE gripper.

soft gripper. Each individual rectangular arm measures 4 mm × 2 mm and has a thickness of 40 μm. As illustrated in Fig. 2e, the resulting four-armed bending structure functions as a gripper, capable of firmly grasping and lifting a 4 mm diameter cotton ball weighing 0.0009 g under UV irradiation (365 nm, 460 mW cm^{-2}). Subsequently, the gripper efficiently releases the ball upon the application of 460 nm (150 mW cm^{-2}) visible light, following the removal of the UV stimulus. This functionality showcases the adaptability and utility of the LCE kirigami design for dynamic manipulation tasks (Movie S2, ESI†).

Curved single-layer kirigami azo-LCE soft actuators

The synergistic encoding of curvilinear geometric properties and alignment microstructures is essential for enriching the LCE deformation patterns, enabling complex deformations of the LCE structure that encompass basic shape variations such as bending, twisting, and dimpling. The intricate nature of the orientation pattern necessitates aligning the cutting geometry with the pattern design to generate intricate deformations, as exemplified in Fig. 3a. When the geometric arms of the kirigami are sickle-shaped, rotational deformation is induced in the azo-LCE kirigami structure. If LC molecules are oriented parallel to the long side of the geometric arms, these four arms undergo bending and rotational deformation (Fig. 3b). Conversely, when the LC molecules in the actuator are dimpling and rotating (Fig. 3c). It is noteworthy that although the microstructural alignment in Fig. 3b is consistent with that of Fig. 2a, the use of distinct geometry patterns leads to significantly different shape transformations. Moreover, while the geometric patterns in Fig. 3b and c are identical, their shape deformations are markedly distinct, dictated by the encoding of differential topological features. Hence, the deformation of kirigami is the result of the interaction of the orientation pattern within the azo-LCE and the specific geometrical design of the sample.

By leveraging the intricate interplay between topological outlines and geometry within kirigami azo-LCE, we can engineer a broader sequence of programmable, intricate 3D shape transformations. Fig. 3d shows the multimodal shape deformation of the wavy four-arm kirigami azo-LCE actuator under different aligned microstructures. Fig. 3e depicts the composite deformation characterized by waving and bending. Fig. 3f illustrates the combined deformation of waving and dimpling. The outcomes reveal that the synergy between orientation modes, kirigami design, and light-driven capabilities gives rise to the showcased undulating shape deformations in azo-LCE films. Notably, the hingeless, monolithic nature of the kirigami design enables a seamless sequence of shape changes (Movie S3, ESI†).

Crawling across solid surfaces necessitates the disruption of frictional symmetry and the application of actuating mechanisms to generate forward motion. However, the inherent limitations of a single rectangular azo-LCE structure prevent it from effectively breaking frictional symmetry and achieving propulsion under UV irradiation. To overcome this challenge, we introduce a sickle-shaped kirigami incision into a single rectangular azo-LCE, thus creating a compliant crawling robot with a distinctive sickle-shaped appendage. This innovation enables the robot to efficiently execute rotary crawling when subjected to UV irradiation. As illustrated in Fig. 3g, the alignment of the LCE kirigami's sickle feature is set perpendicular to its longer side. Upon exposure to UV light (365 nm, 460 mW cm^{-2}), this arrangement induces two simultaneous deformations: rotating and bending movements, accompanied

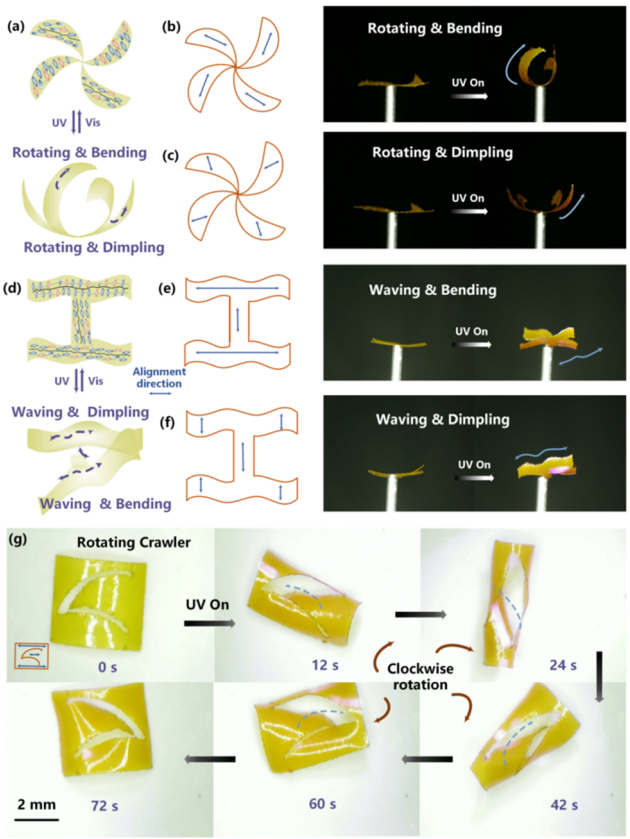

Fig. 3 (a) Multimodal shape morphing of the sickle four-arm kirigami azo-LCE actuator under various alignment microstructures. The superposition deformation of rotating deformation with (b) bending, and (c) dimpling. (d) Multimodal shape morphing of waving a four-arm kirigami azo-LCE actuator under various alignment microstructures. The superposition deformation of waving deformation and (e) bending and (f) dimpling. (g) Rotational crawling motion achieved by a monolith LCE with sickle kirigami geometries.

by the storage of elastic energy. Furthermore, the deformation triggered by UV irradiation results in the continuous release of stored elastic energy, accompanied by a shift in the robot's center of mass. Consequently, this rotational crawling motion effectively disrupts the frictional symmetry, leading to overarching macroscopic locomotion. Repetition of this process ensures sustained rotational crawling. It is noteworthy that the dimensions of the monolith LCE measure 4 mm × 4 mm. The region, which assumes a sickle-shaped configuration, covers an area of 8 mm^2, with the thickness maintaining a constant measurement of 40 μm (Movie S4, ESI†).

Carbonized bilayer kirigami azo-LCE soft actuators

To achieve patterned carbonized layers on kirigami LCE films for localized thermal deformation under light stimulation, we first prepared kirigami azo-LCE films. Then, a 20 μm thick layer of PI tape was applied onto the densely crosslinked surface of the azo-LCE film, followed by scanning PI film using a 450 nm laser engraver. When the scanning speed was fixed at 2.70 mm s^{-1}, we compared the carbonization results at different laser power (Fig. S7, ESI†). It was observed that the carbonized film exhibited non-uniformity at a laser power of 0.45 W, while uniform carbonized films were obtained at power levels of 0.99 W and 1.5 W. However, it is noteworthy that when the power is 1.5 W, the carbonized film tended to peel off during deformation, likely due to the non-uniform thermal expansion caused by excessive laser power. Therefore, a laser power of 0.99 W was selected for carbonization. SEM images of the carbonized film (Fig. 4a and b) revealed distinct graphene layered structures on the film surface. Fig. 4c shows a cross-sectional SEM image of a graphene/azo-LCE bilayer film showing a carbonized layer with a thickness of about 20 μm, an azo-LCE film with a thickness of 40 μm, and an adhesive layer between them with a thickness of about 7 μm, which is not carbonized under laser irradiation. It is worth noting that the pristine PI layer is 12.5 μm while the carbonized layer is about 20 μm, which may be due to the morphological differences in the carbonized layer compared to the PI layer. Fig. S8 (ESI†) shows the cross-sectional morphology of bilayer azo-LCE films before and after laser carbonization. Raman spectroscopy analysis of the graphene layer showed a carbon absorption peak around 800 nm, whereas the PI film did not exhibit carbon absorption peaks (Fig. 4d). Hence, an 808 nm laser was chosen for photothermal experiments, and temperature changes in the graphene film under different laser powers were measured (Fig. S9, ESI†). It was found that the surface temperature of the carbonized layer increased from 35.8 °C to 119 °C when the laser power was increased from 0.22 W to 2.14 W. A laser power of 1.09 W was chosen to give a carbonized layer temperature of 87.6 °C, which was sufficient to actuate the azo-LCE film without causing excessive damage to the film.

The grid structure provides abundant possibilities for localized carbonization, thereby enhancing the diversity of

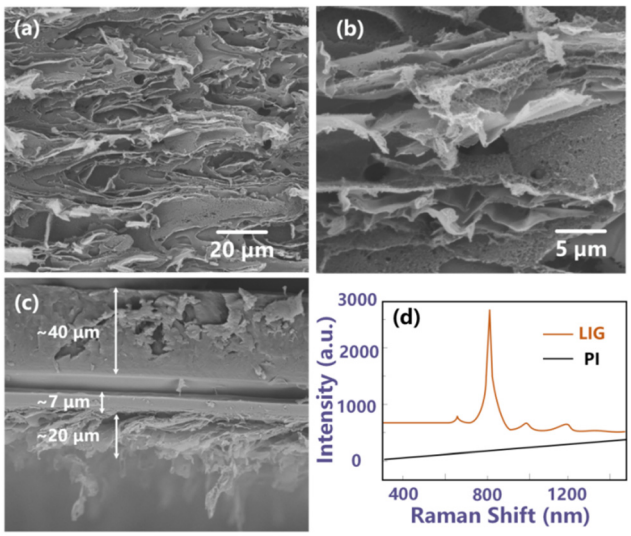

Fig. 4 SEM images at magnifications of (a) 1 K and (b) 4 K showing the graphene morphology formed on carbonized PI films under scanning by a 450 nm laser engraver. (c) Cross-sectional SEM image of the carbonized azo-LCE bilayer film and (d) Raman spectra of the carbonized layer.

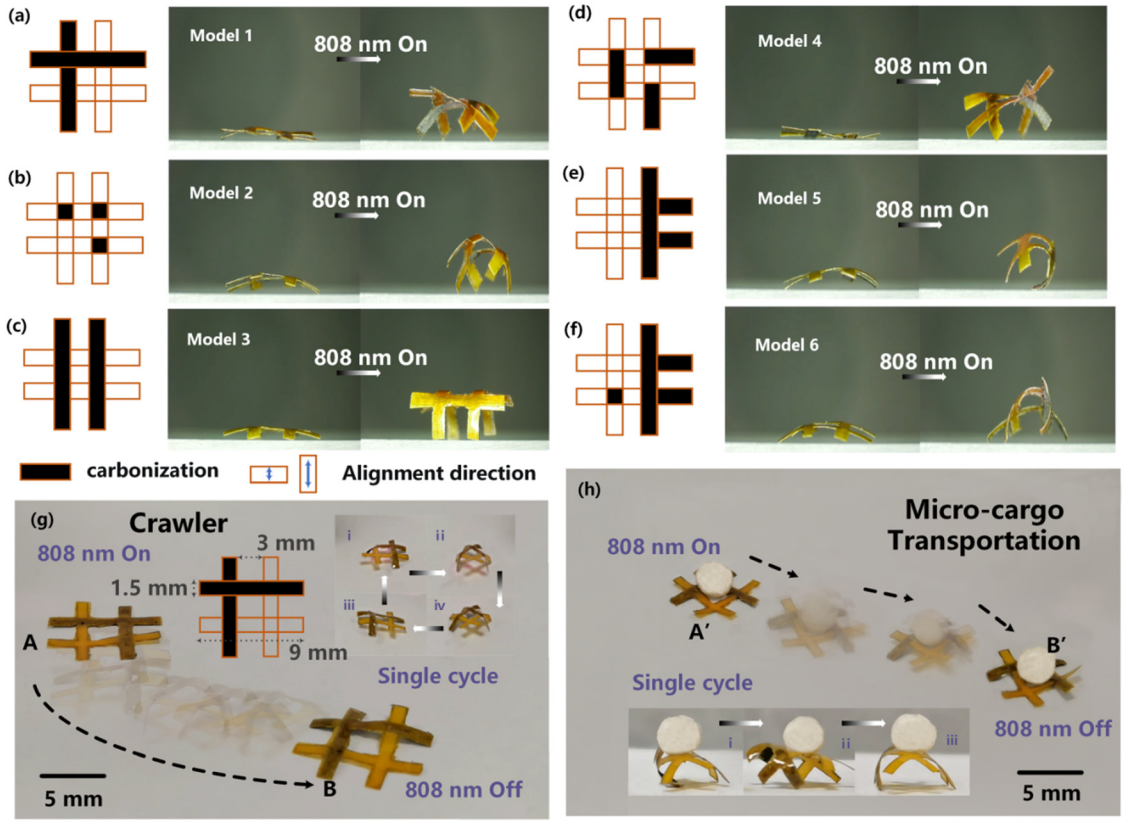

Fig. 5 (a)–(f) The deformation modes exhibited by the bilayer kirigami azo-LCE actuators under six different carbonization schemes. (g) The crawling gait of the bilayer kirigami azo-LCE actuator with grid unit structures featuring cross-bar carbonization, and (h) transporting micro-cargo.

functional designs in azo-LCE. When the structure of the kirigami LCE soft actuator is designed with grid unit shapes and the alignment remains consistent, various local carbonization schemes can be implemented. Effective heating of the carbonized parts leads to localized deformation of the kirigami azo-LCE under 808 nm laser irradiation, resulting in various deformation modes (Fig. 5a–f and Movie S5, ESI†). For instance, carbonization of intersecting vertical stripes causes the actuator to exhibit asymmetric twisting deformation under light (Fig. 5a), while carbonization of adjacent symmetrical vertical stripes results in symmetrical arching deformation (Fig. 5c). Obviously, an actuator that undergoes twisting deformation is well suited for use as a crawler, as this asymmetric force generates the forward force required for crawling motion. As shown in the Fig. 5g (ESI†), the actuator carbonized with an intersecting vertical stripe can move from point A to point B under 808 nm light irradiation. Interestingly, the bilayer kirigami azo-LCE film bends towards this side of the carbonized layer when exposed to 808 nm light, and we hypothesize that the expansion of the carbonized layer is limited by the adhesive layer under the photothermal effect, which generates uneven shear stresses, and these shear stresses are transferred to the azo-LCE layer through the viscoelasticity of the 7 μm adhesive layer, resulting in asymmetric strain distribution. The side strain of the carbonized layer is larger than that of the azo-LCE, which causes the film to bend toward the carbonized layer. Moreover, we demonstrated the use of a crawler actuator to transport micro-cargo by placing a small ball with a diameter of 3.5 mm and a weight of 0.06 g in the central part of the actuator in Fig. 5h. Under the actuating of 808 nm laser irradiation, the actuator transports the microcargo from point A' to point B' (Movie S6, ESI†). It is worth mentioning that the carbonized part is at the intersection of the grid shaped horizontal and vertical stripes, and the actuator exhibits bending deformation similar to that of a flexible actuator centered on a hinge point under light stimulation (Fig. 5b). We speculate that this deformation pattern can be used in applications that require mesh bag-like functionality, such as packaging goods.

Conclusions

In summary, we have demonstrated that a commercial laser engraver operating at 450 nm can be employed to integrate the alignment microstructure and kirigami geometry of azo-LCEs for both single-layer and bilayer configurations. By fine-tuning the engraving parameters, we have achieved precise control over the cutting and alignment templates. This approach has enabled complex deformations such as bending, twisting, and dimpling in a rectangular four-arm kirigami azo-LCE actuator. Notably, transitioning to sickle-shaped and waveform arm designs introduces a superimposition of rotational deformation,

waveform-induced deformation, and foundational deformation, enriching the deformation modes. Additionally, commercial PI films were carbonized into graphene films using the same engraving tool, enabling the fabrication of bilayer kirigami azo-LCE soft actuators with patterned carbonized layers, yielding multiple deformation modes. We demonstrated a method utilizing UV and visible light stimuli to control azo-LCE grippers for grasping and releasing targets. Furthermore, by introducing sickle-shaped kirigami cuts, we created a flexible crawling robot capable of rotational locomotion. Finally, the application of the bilayer actuator in transporting micro-cargoes showcased its effective transportation capability. We envisage the ability to simultaneously irradiate bilayers of patterned azo-LCE with 365 nm and 808 nm beams to drive photochemical and photothermal synergistic deformation, further extending the bilayer LCE actuator deformation mode. Our research highlights the design and fabrication of LCE actuators with multimodal deformation and seamless functional integration through a facile approach, promising broad applications in the field of intelligent soft robots.

Conflicts of interest

The authors declare no conflicting interests.

Data availability

The data supporting this study's findings are available from the corresponding author upon reasonable request.

Acknowledgements

This work is financially supported by the National Key Research and Development Program of China (2022YFA1203700), and the National Natural Science Foundation of China (62475223; 62075186; 624B2121).

References

1 K. Y. Y. Xiao, Z. C. Jiang and Y. Zhao, Liquid Crystal Polymer-Based Soft Robots, *Adv. Intell. Syst.*, 2020, **2**, 000148.
2 C. Ohm, M. Brehmer and R. Zentel, Liquid Crystalline Elastomers as Actuators and Sensors, *Adv. Mater.*, 2010, **22**, 3366–3387.
3 R. S. Kularatne, H. Kim, J. M. Boothby and T. H. Ware, Liquid Crystal Elastomer Actuators: Synthesis, Alignment, and Applications, *J. Polym. Sci., Part B:Polym. Phys.*, 2017, **55**, 395–411.
4 H. Jiang, C. Lia and X. Huang, Actuators based on liquid crystalline elastomer materials, *Nanoscale*, 2013, **5**, 5225.
5 D. D. Sun, J. Z. Zhang, H. P. Li, Z. Y. Shi, Q. Meng, S. R. Liu, J. Z. Chen and X. Y. Liu, Toward Application of Liquid Crystalline Elastomer for Smart Robotics: State of the Art and Challenges, *Polymers*, 2021, **13**, 1889.
6 Z. C. Jiang, Y. Y. Xiao and Y. Zhao, Shining Light on Liquid Crystal Polymer Networks: Preparing, Reconfiguring, and Driving Soft Actuators, *Adv. Opt. Mater.*, 2019, **7**, 1900262.
7 B. Lei, Z. Y. Wen, H. K. Wang, J. Gao and L. J. Chen, Bioinspired Jumping Soft Actuators of the Liquid Crystal Elastomer Enabled by Photo-Mechanical Coupling, *ACS Appl. Mater. Interfaces*, 2024, **16**, 1596–1604.
8 J. H. Sun, W. Liao and Z. Q. Yang, Additive manufacturing of liquid crystal elastomer actuators based on knitting technology, *Adv. Mater.*, 2023, **35**, 2302706.
9 B. Jin, J. Liu, Y. Shi, G. Chen, Q. Zhao and S. Yang, Solvent-Assisted 4D Programming and Reprogramming of Liquid Crystalline Organogels, *Adv. Mater.*, 2022, **34**, 2107855.
10 K. M. Herbert, H. E. Fowler, J. M. McCracken, K. R. Schlafmann, J. A. Koch and T. J. White, Synthesis and alignment of liquid crystalline elastomers, *Nat. Rev. Mater.*, 2022, **7**, 23–38.
11 A. H. Gelebart, D. J. Mulder, G. Vantomme, A. P. H. J. Schenning and D. J. A. Broer, Re-writable, Re-programmable, Dual Light-responsive Polymer Actuator, *Angew. Chem., Int. Ed.*, 2017, **129**, 13621–13624.
12 M. Rogóz, H. Zeng, C. Xuan, D. S. Wiersma and P. Wasylczyk, Light-Driven Soft Robot Mimics Caterpillar Locomotion in Natural Scale, *Adv. Opt. Mater.*, 2016, **4**, 1689–1694.
13 S. Palagi, A. G. Mark, S. Y. Reigh, K. Melde, T. Qiu, H. Zeng, C. Parmeggiani, D. Martella, A. S. Castillo, N. Kapernaum, F. Giesselmann, D. S. Wiersma, E. Lauga and P. Fischer, Structured light enables biomimetic swimmin and versatile locomotion of photoresponsive soft microrobots, *Nat. Mater.*, 2016, **15**, 647–654.
14 F. Ge, R. Yang, X. Tong, F. Camerel and Y. Zhao, Multifunctional Dye-doped Liquid Crystal Polymer Actuator: Light-guided Transportation, Turning in Locomotion and Autonomous Motion, *Angew. Chem., Int. Ed.*, 2018, **57**, 11758–11763.
15 M. Wang, Y. Han, L. Guo, B. Lin and H. Yang, Photocontrol of helix handedness in curled liquid crystal elastomers, *Liq. Cryst.*, 2018, **46**, 1231–1240.
16 M. Lahikainen, H. Zeng and A. Priimagi, Design principles for non-reciprocal photomechanical actuation, *Soft Matter*, 2020, **16**, 5951–5958.
17 O. M. Wani, H. Zeng, H. Wasylczyk and A. Priimagi, Programming Photoresponse in Liquid Crystal Polymer Actuators with Laser Projector, *Adv. Opt. Mater.*, 2018, **6**, 1700949.
18 C. Culbreath, N. Glazar and H. Yokoyama, Automated maskless micro-multidomain photoalignment, *Rev. Sci. Instrum.*, 2011, **82**, 2011.
19 H. Wu, W. Hu, H. Hu, X. Lin, G. Zhu, J. Choi, V. Chigrinov and Y. Lu, Arbitrary photo-patterning in liquid crystal alignments using DMD based lithography system, *Opt. Express*, 2012, **20**, 16684.
20 B. A. Kowalski, V. P. Tondiglia, T. Guin and T. J. White, Voxel resolution in the directed self-assembly of liquid crystal polymer networks and elastomers, *Soft Matter*, 2017, **13**, 4335.
21 H. Aharoni, Y. Xia, X. Y. Zhang, R. D. Kamien and S. Yang, Universal inverse design of surfaces with thin nematic elastomer sheets, *PNAS*, 2018, **28**, 7206–7211.

22 H. Zhu, Y. Wang, Y. Ge, Y. Zhao and C. Jiang, Kirigami-Inspired Programmable Soft Magnetoresponsive Actuators with Versatile Morphing Modes, *Adv. Sci.*, 2022, **9**, 2203711.
23 P. Duhr, Y. A. Meier, A. Damanpack, J. Carpenter, A. R. Studart, A. Rafsanjani and A. F. Demirörs, Kirigami Makes a Soft Magnetic Sheet Crawl, *Adv. Sci.*, 2023, 2301895.
24 Y. Tang, G. Lin, S. Yang, Y. K. Yi, R. D. Kamien and J. Yin, Programmable kiri-kirigami metamaterials, *Adv. Mater.*, 2017, **29**, 1604262.
25 A. Rafsanjani, Y. Zhang, B. Liu, S. M. Rubinstein and K. Bertoldi, Shape-morphing architected sheets with non-periodic cut patterns, *Sci. Rob.*, 2018, **3**, eaar7555.
26 X. Zhang, L. Medina, H. Cai, V. Aksyuk, H. D. Espinosa and D. Lopez, Kirigami Engineering-Nanoscale Structures Exhibiting a Range of Controllable 3D Configurations, *Soft Matter*, 2018, **14**, 9744–9749.
27 M. Zhang, M. Shahsavan, Y. Guo, P. Abdon, Y. Zhang and M. Sitti, Liquid-Crystal-Elastomer-Actuated Reconfigurable Microscale Kirigami Metastructures, *Adv. Mater.*, 2021, 2008605.
28 Y. Cheng, H. Lu, X. Lee, H. Zeng and A. Priimagi, Kirigami-Based Light-Induced Shape-Morphing and Locomotion, *Adv. Mater.*, 2020, **32**, 1906233.
29 A. Rafsanjani and K. Bertoldi, Buckling-Induced Kirigami, *Phys. Rev. Lett.*, 2017, **118**, 084301.
30 Y. Zheng, K. Chen, W. Yang, L. Wu, K. Qu, J. Zhao, T. Jiang and Y. Feng, Kirigami Reconfigurable Gradient Metasurface, *Adv. Funct. Mater.*, 2021, 2107699.
31 X. Zhang, L. Medina, H. Cai, V. Aksyuk, H. D. Espinosa and D. Lopez, Kirigami Engineering-Nanoscale Structures Exhibiting a Range of Controllable 3D Configurations, *Adv. Mater.*, 2020, 2005275.
32 N. An, A. G. Domel, J. Zhou, A. Rafsanjani and K. Bertoldi, Programmable Hierarchical Kirigami, *Adv. Funct. Mater.*, 2020, **30**, 1906711.
33 R. Ma, C. Wu, Z. L. Wang and V. V. Tsukruk, Pop-Up Conducting Large-Area Biographene Kirigami, *ACS Nano*, 2018, **12**, 9714–9720.
34 J. Chen, J. Jiang, J. Weber, G. Vianney and C. Peng, Shape Morphing by Topological Patterns and Profiles in Laser-Cut Liquid Crystal Elastomer Kirigami, *ACS Appl. Mater. Interfaces*, 2023, **15**, 4538–4548.
35 J. C. Chen, Y. T. Cao, J. Y. Pei and H. Y. Zhao, Multifunctional Actuator Based on Graphene/PDMS Composite Materials with Shape Programmable Conffguration and High Photothermal Conversion Capability, *ACS Appl. Mater. Interfaces*, 2023, **15**, 31917–31926.
36 A. S. Kuenstler, Y. Z. Chen, P. O. Bui, H. Kim, A. DeSimone, L. H. Jin and R. C. Hayward, Blueprinting Photothermal Shape-Morphing of Liquid Crystal Elastomers, *Adv. Mater.*, 2020, **32**, 2000609.
37 J. Lin, Z. W. Peng, Y. Y. Liu, F. Ruiz-Zepeda, R. Q. Ye, E. L. G. Samuel, M. J. Yacaman, B. I. Yakobson and J. M. Tour, Laser-induced porous graphene films from commercial polymers, *Nat. Commun.*, 2014, **5**, 5714.
38 J. D. Xu, R. S. Li, S. R. Ji, B. C. Zhao, T. R. Cui, X. C. Tan, G. Y. Gou, J. M. Jian, H. K. Xu, Y. C. Qiao, Y. Yang, S. Zhang and T. L. Ren, Multifunctional Graphene Microstructures Inspired by Honeycomb for Ultrahigh Performance Electromagnetic Interference Shielding and Wearable Applications, *ACS Nano*, 2021, **15**, 8907–8918.
39 Y. Kim, S. Park, B. Kim, W. J. Park and H. J. Kim, Laser lift-off of polyimide thin-fflm from glass carrier using DPSS laser pulses of top-hat square proffles, *Opt. Laser Technol.*, 2021, **142**, 107245.
40 H. W. Liu, K. S. Chen, R. M. Wu, S. S. Pan and C. Y. Zhang, Laser-Induced Graphene-based Flexible Substrate with Photothermal Conversion and Photoresponse Performance on Polyimide Film, *ACS Appl. Mater. Interfaces*, 2023, **15**, 46550–46558.
41 B. Lei, H. K. Wang, K. H. Wu, J. Gao and L. J. Chen, Lightdriven Folding Liquid Crystal Elastomer Catapult with Improved Morphing Velocity, *Adv. Intell. Syst.*, 2023, **5**, 2200360.

